energies

MDPI

Article

Application and Verification of Formation Pressure Estimation for Geo-Energy Engineering Based on Flow Regime Identification Analysis of Different Injection/Shut-In Tests

Qiuyang Xu [1,2], Yuehui Yang [1,*], Awei Li [1], Bangchen Wu [1], Hao Zhang [1], Ran Li [1], Shiyuan Li [2], Chongyuan Zhang [1], Qunce Chen [1] and Dongsheng Sun [1]

[1] Institute of Geomechanics, Chinese Academy of Geological Sciences, Beijing 100081, China; qiuyang_xu27@163.com (Q.X.); 13811547672@163.com (A.L.); wubangchen@mail.cgs.gov.cn (B.W.); zhhao@cags.ac.cn (H.Z.); liran9112@163.com (R.L.); zhchongyuan@126.com (C.Z.); chenqunce@sina.com (Q.C.); dongshengsun@cags.ac.cn (D.S.)

[2] School of Petroleum Engineering, China University of Petroleum, Beijing 102249, China; lishiyuan1983@cup.edu.cn

* Correspondence: yangyuehui@mail.cgs.gov.cn

Abstract

Conventional Diagnostic Fracture Injection Tests (DFITs) are widely used for formation pressure estimation, but in practice, they frequently require days, weeks, or even months of extended shut-in periods, a challenge particularly pronounced when large injection volumes are coupled with ultra-low formation permeability. While recent studies have proposed various modified DFIT approaches to reduce testing time, direct physical validation confirming the reliability of the derived formation pressure estimates remains scarce in the literature. This study applies a low-rate/volume injection mini-frac approach that integrates flow regime identification and Horner analysis. Two complementary field cases are presented: a standard DFIT in a shale reservoir to validate the baseline methodology, and a low-volume mini-frac in a tight granite formation to demonstrate rapid estimation. Results show that low-volume injections exhibit a flow regime evolution identical to standard DFITs, yet this approach is expected to accelerate the transition to the pseudo-radial flow regime. To verify the reliability of formation pressure estimates derived from such methods, the formation pressure estimated in the low-rate/volume injection mini-frac case was benchmarked against a decade of continuous downhole fluid pressure monitoring data from the same well, yielding a relative error of less than 5%. The findings suggest that employing a lower injection rate and volume can improve formation pressure testing efficiency, with potential applications in unconventional hydrocarbon development and deep geo-energy engineering.

Keywords: formation pressure; geo-energy; flow regime identification; Horner time; mini-frac test; pseudo-radial flow

Check for updates

Academic Editor: Dameng Liu

Received: 11 March 2026
Revised: 28 April 2026
Accepted: 15 May 2026
Published: 19 May 2026

Copyright: © 2026 by the authors. Licensee MDPI, Basel, Switzerland. This article is an open access article distributed under the terms and conditions of the Creative Commons Attribution (CC BY) license.

1. Introduction

Pore pressure represents the fluid pressure within the pore spaces of porous rocks. Since the mid-1960s, when abnormally high pore pressure (overpressure) was encountered in U.S. drilling operations, the phenomenon has drawn extensive attention across the rock mechanics and structural geology communities [1,2]. Accurately determining pore pressure is a prerequisite for safe and economic hydrocarbon exploration and development. In unconventional reservoirs, overpressure typically signals favorable preservation

conditions and is critical for identifying sweet spots [3–5]. During reservoir stimulation, pore pressure directly dictates the effective stress state and fracture pressure gradient, making it a core parameter for optimizing volume fracturing designs and fracture network morphology [6]. Furthermore, in deep fluid injection and extraction projects—such as geothermal energy extraction and underground gas storage—formation stability is closely tied to the pore pressure state. Fluid injection increases pore pressure and reduces effective normal stress, thereby elevating the risk of fault shear instability. Consequently, accurate pore pressure data is essential for defining safe operating windows and assessing induced seismicity risks [7–9]. Therefore, rapidly and accurately determining pore pressure is of great engineering and practical importance.

Current strategies for constraining formation/pore pressure can be grouped into two complementary paradigms: prediction and in situ measurement. Prediction infers pore pressure from seismic and logging observables (e.g., velocity, resistivity, and acoustic transit time) through empirical compaction trends or rock-physics relationships, offering cost-effective, spatially extensive characterization that supports early-stage risk screening and well design [10–13]. Nevertheless, such predictions are intrinsically assumption-sensitive and may incur systematic bias where lithologic heterogeneity, diagenetic overprint, unloading, compartmentalization, or mixed overpressure mechanisms invalidate a single transferable trend. In contrast, the mini-frac is a widely used in situ method for determining in situ stress, formation pressure, and permeability [14]. As a direct observation of formation seepage characteristics, mini-frac results are generally considered highly reliable. Early work by Nolte established the G-function analysis based on the Carter leak-off model, laying the theoretical foundation for inverting fracture geometry and closure pressure from falloff data [15]. Determining formation pressure, however, requires analyzing the pressure falloff after the fracture has completely closed. Soliman and Craig and Blasingame integrated Pressure Transient Analysis (PTA) into After-Closure Analysis (ACA), revealing that post-closure pressure decay is governed by the transient seepage mechanisms of the porous media [16–19]. This framework enables the estimation of formation pressure by identifying the transition from linear to pseudo-radial flow and extrapolating pressure data to infinite time using Horner or superposition time functions [20–23].

Nevertheless, the practical application of this technology is constrained by two main factors. First, rigorous validation of these formation pressure estimates against independent, long-term monitoring data remains scarce in the literature. Second, injecting large fluid volumes at high rates creates a large radius of investigation. This necessitates extended shut-in periods for pressure diffusion and re-equilibration. In practice, these periods often span days, weeks, or even months, resulting in significant operational inefficiency, particularly in unconventional reservoirs. These limitations have hindered broader adoption of the technology, raising the critical question of whether reducing volume compromises the fidelity of the inferred formation pressure. Consequently, recent studies have increasingly focused on optimizing test designs and improving interpretation models to overcome these practical constraints [24,25].

This study applies a low-volume mini-frac approach for efficient formation pressure estimation. The paper first details the testing procedures and the theoretical basis of flow regime identification and Horner analysis. The methodology is then validated through two complementary field cases: a standard DFIT in a shale reservoir (Case 1) to establish the baseline, and a low-volume mini-frac in a tight granite formation (Case 2) to demonstrate rapid estimation. Notably, the estimation results are rigorously verified against a decade of continuous monitoring data. The applicability and future optimization directions of this approach are then systematically discussed, offering a practical reference for implementing low-volume formation pressure testing in field operations.

2. Methods and Procedures

2.1. Brief of Mini-Frac Test

Hydraulic fracturing tests with limited fluid volumes are collectively known as mini-frac tests—a diagnostic category distinct from large-scale reservoir stimulation. Among these, the Diagnostic Fracture Injection Test (DFIT) is a conventional method typically performed with a single injection at relatively high rates (300–1500 L/min) [26]. In contrast, the mini-frac test in Case 2 of this study employed a strictly limited fluid volume and a significantly lower rate (10–100 L/min) to initiate only micro-fractures. Even so, the resulting fractures should extend to a distance of at least 3–5 borehole radii, which is sufficient to penetrate beyond the stress-altered near-wellbore zone. Following a brief shut-in period to allow for natural pressure decay, pumping was resumed to reopen the fractures. This injection/shut-in sequence was cycled to record the breakdown pressure during the initial cycle and reopening pressures in subsequent cycles [14]. The theoretical pressure response curve is illustrated in Figure 1. Crucially, this study extended the shut-in duration of the last reopening cycle. Downhole memory gauges were deployed to capture a complete dataset of pressure falloff, spanning both pre- and post-closure periods, for flow regime identification. By isolating falloff data corresponding to specific flow regimes, formation pressure parameters were estimated through regression analysis against the appropriate time functions and subsequent extrapolation [16,19].

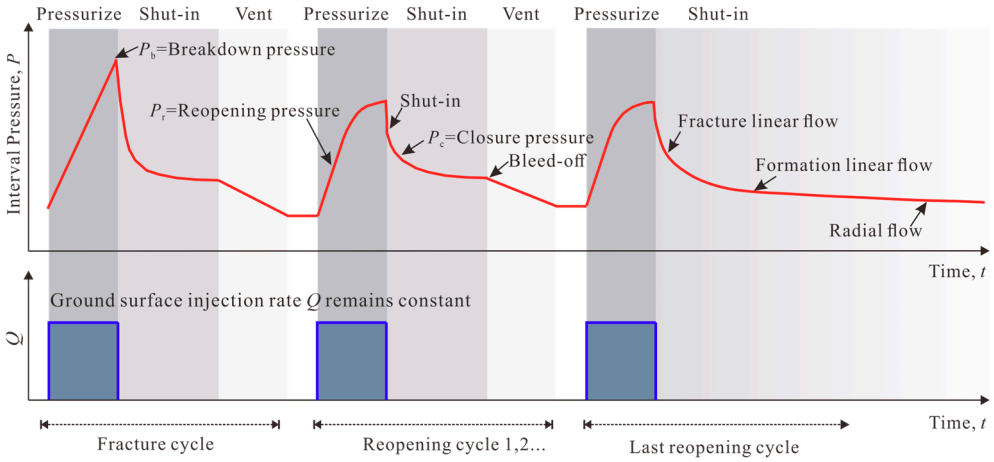


Figure 1. The idealized curve in mini-frac tests shows the interval pressure (P) and surface injection flow rate (Q) during the initial fracturing and subsequent refrac cycles. The curve is divided into three distinct phases: Pressurization (Injection), Shut-in (Pressure decay due to leak-off), and Vent, each highlighted by different background colors to differentiate the stages. The interval pressures indicated are those at breakdown pressure (P_b), re-opening pressure (P_r), and closure pressure (P_c). The extended shut-in curve from the last reopening cycle is utilized for flow regime identification.

2.2. Flow Regime Identification

Fundamentally, pressure falloff data recorded during the shut-in period reflect the fluid seepage process within the formation. As illustrated in Figure 2, distinct slope characteristics observed on flow regime identification plots correspond to specific fluid flow states occurring at different stages. Accurate identification of the flow regimes governing the pressure falloff is a critical component of DFIT data analysis, serving as the basis for all subsequent quantitative estimations of formation and fracture parameters [18]. This study applies flow regime identification techniques derived from PTA to pressure falloff data acquired during extended shut-in periods to analyze the distinct flow stages throughout the pressure decline process.

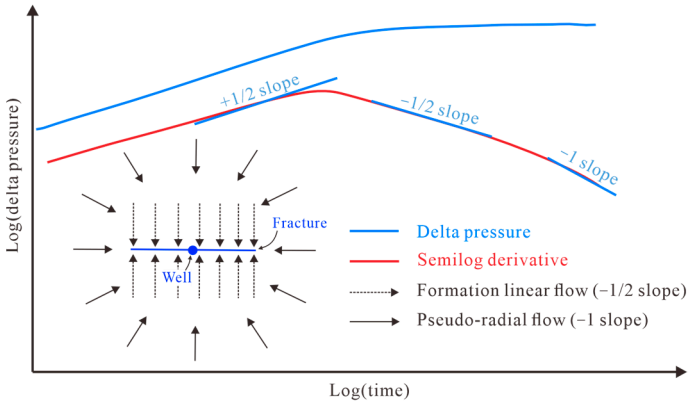


Figure 2. Theoretical framework of after-closure flow regime analysis. Schematic representations of fluid seepage states at different stages: formation linear flow, and pseudo-radial flow. The corresponding theoretical flow regime identification curves on log-log coordinates. The blue curve represents the pressure change (ΔP) with respect to shut-in time. The red curve represents the semilog derivative of pressure with respect to shut-in time, highlighting distinct flow regimes based on slope characteristics: the $+1/2$ slope typically indicates fracture closure (although its signature may not always be evident), the $-1/2$ slope corresponds to formation linear flow, and the -1 slope corresponds to pseudo-radial flow. Crucially, this final regime provides the reliable pressure falloff data necessary for accurate formation pressure estimation.

The theoretical basis for flow regime identification lies in the fact that different flow regimes exhibit distinct pressure and pressure derivative characteristics on log-log plots. The pressure derivative is highly sensitive to changes in flow conditions; consequently, its shape serves as the decisive criterion for flow regime identification [26,27].

Equations (1) and (2) describe the relationship between pressure change and time for the formation linear flow and pseudo-radial flow regimes, respectively [16]. The detailed derivations are provided in Appendix A.

$$\Delta P(t) = \frac{V_{inj}}{2A_f}\sqrt{\frac{\mu}{\pi k \phi c_t}} \cdot t^{-1/2} \tag{1}$$

$$\Delta P(t) = \frac{V_{inj}\mu}{4\pi kh} \cdot t^{-1} \tag{2}$$

where ΔP is the formation pressure change; V_{inj} is the injected volume; A_f is the fracture surface area; t is the natural time; k is the permeability; ϕ is the porosity; μ is the fluid viscosity; c_t is the total compressibility; and h denotes the effective formation thickness.

A comparison of these two equations reveals that once the formation fluid enters the pseudo-radial flow regime, the pressure change becomes independent of the hydraulic fracture scale. Consequently, it is theoretically feasible to estimate formation pressure using post-closure falloff data derived from micro-fractures created during mini-frac tests.

2.3. Formation Pressure Estimation Method

Accurately estimating formation pressure using post-shut-in falloff data is a critical component of ACA. This step is essential for calculating reservoir permeability, assessing stress states, and optimizing fracturing designs [18]. Among various interpretation methods, the Horner analysis is widely regarded as reliable [20].

This approach estimates formation pressure by extrapolating pressure falloff data against Horner time [16,21]. Its reliable application requires that the analyzed data fall within a well-developed infinite-acting pseudo-radial flow regime, which is the key implicit assumption of the Horner method. Two fundamental prerequisites must therefore be satisfied: first, the pressure response must exhibit a sufficiently developed pseudo-radial

flow behavior; second, the selected analysis interval should not be significantly affected by boundary effects, wellbore storage, leakoff, or other non-reservoir factors.

The method correlates the falloff data with a dimensionless time function, Horner time (T_h), defined as:

$$T_h = \frac{t_P + \Delta t}{\Delta t} \tag{3}$$

where t_P is the injection time and Δt is the shut-in time.

In a Horner plot, bottomhole pressure is plotted on a Cartesian y-axis against Horner time on a logarithmic x-axis. The pseudo-radial flow regime appears as a distinct linear segment, whose slope is directly proportional to the formation flow capacity. Extrapolating this linear trend to $T_h = 1$—which corresponds to infinite shut-in time ($\Delta t \to \infty$), yields the estimated formation pressure at the y-intercept. This point represents the condition when all injection-induced pressure perturbations have fully dissipated and formation pressure has returned to its initial, equilibrium state.

3. Field Case Studies

This section presents two field applications. Case 1 demonstrates the application of flow regime theory in a standard DFIT context within a shale reservoir, establishing the baseline evolution of post-closure flow regimes under conventional operational parameters. Building upon this established reference, Case 2 illustrates a low-rate/volume injection mini-frac in a granite formation, where long-term monitoring data serve as a benchmark for method validation.

The operational configurations for both cases are detailed in Table 1. Case 1 was conducted in a cased horizontal interval within a shale formation at a depth of 2528 m. A fracturing unit injected approximately 5 m^3 of clear water at a rate of 500 L/min for 10 min. Pressure variations throughout the test were recorded by a wellhead pressure gauge with a sampling frequency of 1 Hz. Case 2 involved an open-hole vertical interval in a granite formation at a depth of 625 m. A surface plunger pump was utilized to inject roughly 0.018 m^3 of clear water at a rate of 18 L/min for a duration of 1 min. High-frequency pressure data were recorded at 1 Hz using both wellhead and downhole gauges to monitor the full pressure history.

Table 1. Test configurations for the field cases.

Parameter	Case 1	Case 2
Test depth (m)	4580 (TVD = 2528)	625
Lithology	Shale	Granite
Completion method	Cased hole	Open hole
Wellbore geometry	Horizontal	Vertical
Wellbore diameter	139.7 mm	76 mm
Injection fluid	Clear water	Clear water
Injection rate (L/min)	~500	~18
Injection duration (min)	~10	~1
Sampling frequency (Hz)	1	1

3.1. Case 1

In the evaluation of unconventional resources, the DFIT is extensively applied for formation parameter inversion. Case 1 involves a horizontal well deployed in a typical shale gas reservoir. A DFIT was conducted on this well to determine formation pressure and other formation parameters, optimize the fracturing and gas testing design, and provide a reliable basis for productivity evaluation.

The test interval was located at the toe of the horizontal section and isolated using a toe sliding sleeve system, with a wellhead pressure gauge installed to record pressure variations. Using a toe valve is considered the best practice for DFITs, as it ensures the test is conducted on a formation with no prior injection history. This precludes the risk of injecting into a previously created fracture, which would otherwise distort the geometry of the pressure transient. During the test, a fracturing unit injected clear water at a rate of 500 L/min until formation breakdown occurred. Injection continued for several minutes before the well was shut in for an extended period to acquire pressure falloff data reflecting reservoir transient behavior. Figure 3 illustrates the DFIT curve for Case 1, which had a shut-in duration of approximately 427 h.

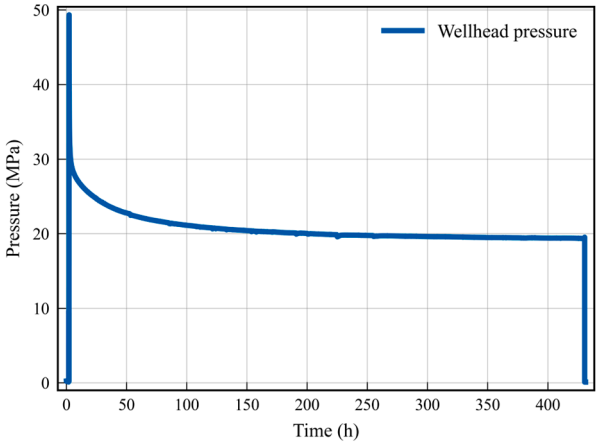


Figure 3. Wellhead pressure response curve of DFIT for Case 1.

Subsequently, flow regime identification was performed on the pressure falloff data to characterize the typical evolution of flow regimes during the DFIT. The corresponding log-log diagnostic plot is presented in Figure 4.

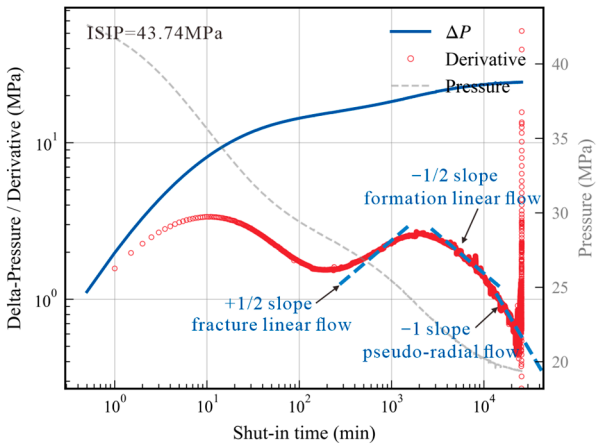


Figure 4. Flow regime identification analysis of Case 1 pressure falloff data. The red curve represents the pressure derivative, the blue curve depicts the delta-pressure and the grey curve illustrates the raw pressure falloff profile following shut-in.

To mitigate the severe noise often observed in late-time pressure derivatives calculated via simple differentiation, the Bourdet derivative algorithm—a standard technique in PTA as described in Appendix B—was applied to generate the diagnostic curves. The analysis identifies the emergence of fracture linear flow approximately 74.8 h after shut-in, with the transition to pseudo-radial flow occurring at roughly 213 h.

Analysis of the Case 1 data reveals a characteristic evolution of flow regimes following pump shut-in. Although the initial +1/2 slope phase signifying fracture linear flow is subtle, the derivative slope shifts to negative values as the pressure transient propagates into the far field, clearly exhibiting a distinct −1/2 slope characteristic of formation linear flow before eventually evolving into the −1 slope of pseudo-radial flow.

Consequently, the pressure falloff data corresponding to the pseudo-radial flow regime were isolated and regressed against Horner time, as shown in Figure 5.

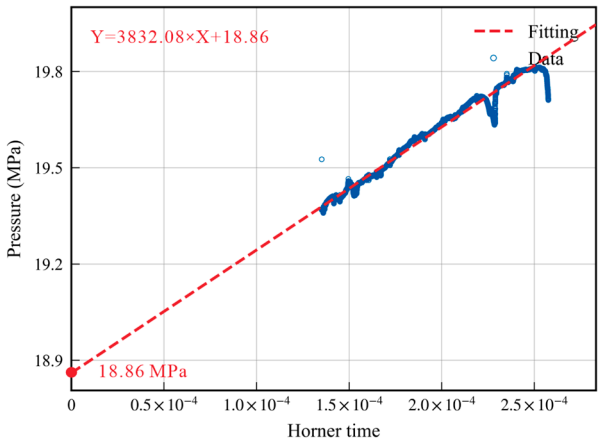


Figure 5. Regression and extrapolation of pseudo-radial flow pressure falloff data against Horner time for Case 1.

The hydrostatic pressure (P_h) of the static fluid column is determined by $P_h = \rho_w g h$, where ρ_w is the density of the injected clear water (1000 kg/m^3), g is the gravitational acceleration (10 m/s^2), and h is the true vertical depth of the test interval (2528 m). Applying these parameters results in a hydrostatic pressure of 25.28 MPa, Consequently, summing the extrapolated surface pressure (18.86 MPa) and the hydrostatic pressure (25.28 MPa) yields a formation pressure of 44.14 MPa.

The conversion from wellhead pressure to bottomhole pressure can be influenced by friction losses, hydrostatic effects, thermal effects, and wellbore-related transient distortion. Friction-related effects are dynamic and dissipate rapidly after shut-in as the flow rate approaches zero [14,24]. Wellbore storage mainly distorts the early-time pressure response and is generally reduced before the late-time pseudo-radial flow regime is established [28,29]. For the hydrostatic correction, elevated downhole pressure compresses the wellbore fluid, increases its density, and may lead to a slight underestimation of bottomhole and formation pressure if a constant surface density is assumed. In contrast, geothermal heating thermally expands the fluid, reduces its density, and may result in a marginal overestimation. Because pressure compression and thermal expansion affect fluid density in opposite directions, their effects may partially offset each other.

Therefore, these complex factors are expected to exert only a limited influence on the conversion from wellhead pressure to bottomhole pressure. When a refined formation pressure estimate is required, the net correction should be quantified using downhole pressure-temperature profiles, with the pressure- and temperature-dependent fluid density evaluated from the fluid compressibility and volumetric thermal expansion coefficient.

3.2. Case 2

Case 2 involves an experimental open-hole vertical well located in an area characterized by simple geological structure and flat terrain. The rock mass consists of homogeneous, intact granite [30]. The test interval depth was determined through a comprehensive analy-

sis of core samples and ultrasonic imaging logs to strictly avoid intersecting pre-existing natural fractures.

Building on the flow regime theory validated in Case 1, a mini-frac test was performed on this well to obtain in situ pressure falloff data for ACA. The test interval was isolated using an open-hole straddle packer system with a 1.5 m spacing. Clear water was used as the fracturing fluid, while both downhole memory gauges and surface gauges were installed to continuously monitor pressure. The formation was broken down using a low-rate/volume injection strategy. After completing several injection-falloff cycles, the well underwent an extended shut-in period to acquire data reflecting the formation's transient behavior. Data processing follows the same methodology as DFITs: flow regimes are identified via log-log diagnostic plots, the pseudo-radial flow phase is isolated, and Horner analysis is applied to regress and extrapolate the data to estimate formation pressure. Figure 6 displays the injection-falloff profile for the last reopening cycle, which included a shut-in duration of approximately 4 h.

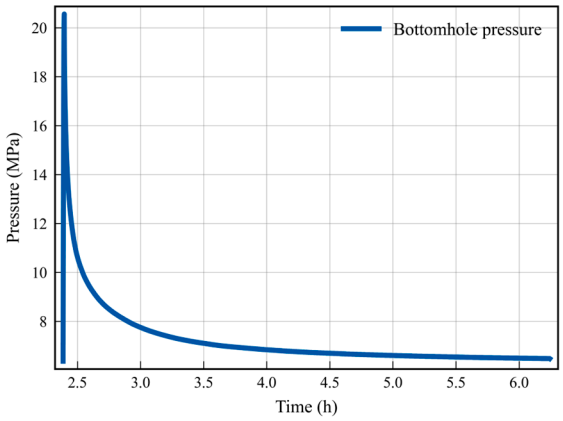


Figure 6. Bottomhole pressure response curve of last reopening cycle for Case 2.

Pressure falloff data acquired during the extended shut-in period were analyzed to identify flow regimes, as shown in Figure 7.

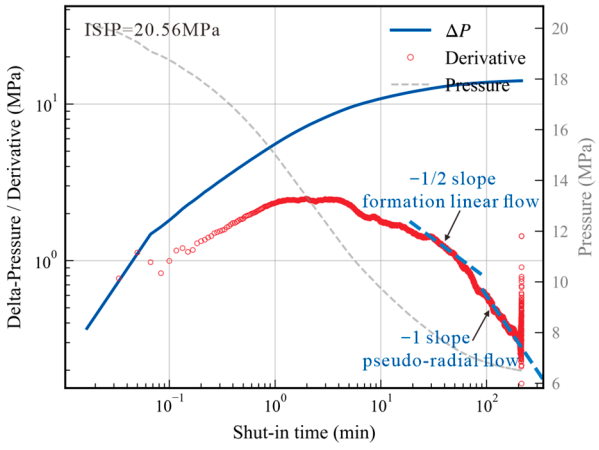


Figure 7. Flow regime identification analysis of the pressure falloff data from the last reopening cycle in Case 2. The red curve represents the pressure derivative, the blue curve depicts the delta-pressure and the grey curve illustrates the raw pressure falloff profile following shut-in.

As indicated by the diagnostic plot, the post-closure flow regime evolution for the low-rate/volume injection mini-frac is identical to that of a standard DFIT. Both are characterized by an initial formation linear flow with a slope of $-1/2$, followed by a transition to

pseudo-radial flow with a slope of −1 during the late pressure falloff stage. The log-log diagnostic plot indicates the onset of formation linear flow approximately 0.6 h after shut-in, followed by a transition to pseudo-radial flow at roughly 2 h.

Subsequently, the pressure falloff data within the pseudo-radial flow regime—identified via the flow regime analysis—were isolated and regressed against Horner time. Extrapolating the fitted line yielded a formation pressure of 6.23 MPa, as shown in Figure 8.

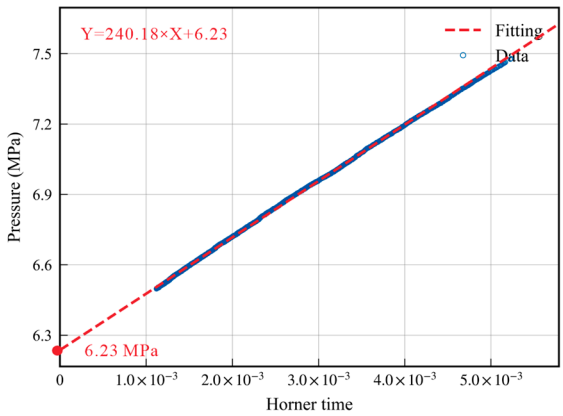


Figure 8. Regression and extrapolation of pseudo-radial flow pressure falloff data against Horner time for the last reopening cycle of Case 2.

Continuous monitoring over the past decade shows that the static water level in this borehole exhibits minimal fluctuation, indicating stable regional hydrogeological conditions (Figure 9). Given this stability and interpreting the local aquifer as a well-connected confined system, the initial formation pressure at the test interval can be reliably calculated as the hydrostatic pressure corresponding to this static water level. Consequently, the estimated formation pressure of 6.23 MPa aligns closely with this benchmark value of 6.10 MPa, corresponding to a relative deviation of approximately 2.13%, which is within 5%.

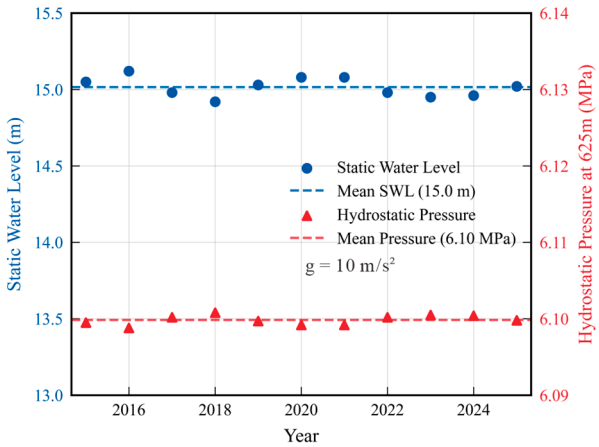


Figure 9. Decade-long variation history of static water level and the corresponding baseline formation pressure (equivalent hydrostatic pressure) at the test depth of 625 m for Case 2. The dashed lines represent the mean values over the monitoring period (Mean SWL = 15.0 m; Mean Pressure = 6.10 MPa).

Direct benchmarking of DFIT-derived formation pressure estimates against long-term, independent monitoring data from the same well remains scarce in the literature. Published results indicate that when DFIT data do not reach a clean after-closure impulse signature, approximate pore pressure estimates derived from truncated data can carry uncertainties on the order of ±600 psi (±4.14 MPa), as reported by McClure et al. [31] from a statistical analysis of 62 DFITs across nine shale plays. By contrast, the close

agreement obtained in Case 2 (relative error of 2.13%, corresponding to ~0.13 MPa) reflects the rigorous identification of pseudo-radial flow prior to Horner extrapolation and the use of high-precision downhole memory gauges, both of which minimize potential sources of systematic bias.

To evaluate the sensitivity of the Horner extrapolation to the choice of data interval within the pseudo-radial flow regime, the analysis was repeated using three progressively truncated data segments, with cutoff pressures of 6.85 MPa, 6.72 MPa, and 6.67 MPa, respectively (i.e., the initial pressures of the pseudo-radial flow intervals; see Figure 7). The corresponding Horner-extrapolated formation pressures are 6.24 MPa, 6.23 MPa, and 6.23 MPa, respectively. The maximum variation among these estimates is 0.01 MPa, confirming that the pore-pressure estimate is insensitive to the specific selection of data points within the identified pseudo-radial flow window.

4. Discussion

The estimation of formation/pore pressure via the low-rate/volume injection mini-frac technique discussed in this study essentially applies pressure transient analysis (PTA) to falloff data acquired from the last reopening cycle. The time required to reach pseudo-radial flow is governed depends on both test design parameters and intrinsic formation properties. Regarding test design, Equation (2) indicates that the required shut-in time scales positively with injected volume ($t_{radial} \propto V_{inj}$); a significantly reduced injection volume therefore accelerates pressure equilibration and minimizes the pressure perturbation radius. Regarding formation properties, hydraulic diffusivity—governed by permeability, porosity, and system compressibility—dictates the intrinsic pressure diffusion rate. In Case 2, pseudo-radial flow emerged within approximately 2 h, demonstrating the rapid equilibration achievable with minimal injection volume in the tested tight granite formation.

The two field cases serve distinct, non-comparative functions. Case 1 validates the fundamental flow-regime identification and Horner analysis methodology in an ultra-low permeability shale under standard DFIT conditions. Case 2 provides an independent demonstration that a low-volume injection test in tight granite can yield a reliable formation pressure estimate within a short timeframe—a result corroborated by decade-long monitoring data.

The theoretical basis of this methodology rests on the porous-media diffusion equation and therefore extends, in principle, to other permeable lithologies. A clear limitation, however, is that the present study relies on two cases that differ substantially in lithology, depth, permeability, and wellbore configuration. Consequently, the rapid equilibration observed in Case 2 cannot be directly compared with Case 1 to isolate the independent effect of injection volume. Systematic validation incorporating a broader statistical sample under strictly controlled, single-variable experimental designs is needed to quantitatively decouple the individual contributions of injection volume and specific formation properties.

In field applications, however, the hydraulic fractures created by low-rate/volume injection tests are significantly smaller in scale than those in standard DFITs. This renders the +1/2 slope line characteristic of fracture linear flow much less distinct on the pressure derivative curve compared to DFITs. To address this, we recommend using G-function analysis and the recently proposed Total System Stiffness (TSS) method to rigorously identify the closure pressure and closure time [32–36]. Published studies indicate that in some cases flow-regime diagnostics may identify a "false radial" signature—i.e., one that does not correspond to genuine radial flow [28,37]. This approach ensures data used for Horner plotting comes strictly from the after-closure phase. The small injection volume restricts the pressure perturbation radius within the homogeneous, intact granite formation, thereby maintaining an infinite-acting flow regime. The close agreement between the estimated

formation pressure and the independent decade-long monitoring benchmark confirms that the 4 h shut-in duration did not introduce systematic bias into the extrapolation. Furthermore, high-quality pressure falloff data are essential for accurately identifying flow regimes and obtaining reliable interpretation results. During data processing, the Bourdet derivative algorithm was employed to effectively suppress the data fluctuations induced by numerical differentiation.

5. Conclusions

Post-closure pressure falloff data derived from micro-fractures created by low-rate/volume injection exhibit flow regime evolution characteristics consistent with those observed in standard DFITs. Specifically, the flow regime progresses from formation linear flow to pseudo-radial flow.

Estimating formation pressure using pressure falloff data acquired from the last reopening cycle of a low-rate/volume injection mini-frac is both theoretically and practically feasible. Provided that the falloff data display distinct pseudo-radial flow characteristics after fracture closure on the log-log diagnostic plot, reliable formation pressure parameters can be obtained by regressing the data from the pseudo-radial flow regime against the Horner time function and extrapolating the trend.

Field measurements from scientific boreholes demonstrate that the formation pressure estimated using this method is consistent with baseline values, yielding a relative error of less than 5%. This indicates practical utility regarding testing time and diagnostic accuracy. Although the current validation is restricted to granite, the methodology is fundamentally based on porous media diffusion theory, suggesting applicability in other low-permeability formations, including shale, sandstone, and limestone. Conversely, this method is less suitable for high-permeability formations. The challenge in such formations lies not only in the need for substantially higher injection rates or volumes, but more importantly in the fact that rapid pressure dissipation generally prevents objective identification of flow regimes during pressure transient analysis.

Author Contributions: Conceptualization, Y.Y.; methodology, Q.X., Y.Y. and Q.C.; software, Q.X. and Y.Y.; validation, Y.Y., R.L., B.W. and A.L.; formal analysis, D.S., Q.X. and Y.Y.; investigation, D.S., Q.X. and B.W.; resources, D.S. and Y.Y.; data curation, Y.Y., A.L. and R.L.; writing—original draft preparation, Q.X.; writing—review and editing, D.S., Y.Y., H.Z., S.L. and C.Z.; visualization, Q.X.; supervision, D.S. and Y.Y.; project administration, D.S., C.Z. and A.L.; funding acquisition, D.S. and Y.Y. All authors have read and agreed to the published version of the manuscript.

Funding: This study was supported by the Deep Earth Probe and Mineral Resources Exploration-National Science and Technology Major Project (No. 2024ZD1000701), the Oil & Gas Major Project (2025ZD1401401), and the Central Public-interest Scientific Institution Basal Research Fund (No. DZLXJK202407).

Data Availability Statement: The data presented in this study are available on request from the corresponding author (yangyuehui@mail.cgs.gov.cn).

Acknowledgments: We sincerely thank the reviewers for their valuable comments and the technical staff for their dedicated efforts and close cooperation during the field experiments.

Conflicts of Interest: The authors declare no conflicts of interest.

Abbreviations

The following abbreviations are used in this manuscript:

DFIT	Diagnostic Fracture Injection Test
PTA	Pressure Transient Analysis
ACA	After-Closure Analysis
SWL	Static Water Level
TSS	Total System Stiffness

Appendix A

If the wellbore and hydraulic fracture are modeled as a single, connected system, the flow of formation fluid through the porous medium is described by the diffusion equation [38]. For a homogeneous, isotropic formation containing a slightly compressible fluid, this governing equation takes the form:

$$\nabla^2 P = \frac{1}{\eta}\frac{\partial P}{\partial t} \tag{A1}$$

where η represents the hydraulic diffusivity, defined as:

$$\eta = \frac{k}{\phi \mu c_t} \tag{A2}$$

During the early post-closure period, the propagation distance of the pressure transient is significantly smaller than the fracture length. At this stage, the fracture behaves as an infinite plane relative to the fluid in its vicinity, resulting in flow that is predominantly perpendicular to the fracture face (defined here as the x-direction) [15]. Consequently, the governing equation reduces to a one-dimensional form:

$$\frac{\partial^2 P}{\partial x^2} = \frac{1}{\eta}\frac{\partial P}{\partial t} \tag{A3}$$

According to the theory of partial differential equations [39], the fundamental solution for an instantaneous plane source of strength released at $x = 0$ and time $t = 0$ within an infinite medium is expressed as:

$$\Delta P(t) = \frac{S_{plane}}{2\sqrt{\pi \eta t}} exp\left(-\frac{x^2}{4\eta t}\right) \tag{A4}$$

where S_{plane} represents the plane source strength, related to the volume of fluid injected per unit fracture area, defined as:

$$S_{plane} = \frac{V_{inj}/A_f}{\phi c_t} \tag{A5}$$

For the bottomhole pressure response at the fracture face (as x approaches 0), the exponential term $exp(0)$ approaches 1. Substituting the source strength S_{plane} and the diffusivity η into the equation, and consolidating the constant terms, the solution for bottomhole pressure is obtained as:

$$\Delta P(t) = \frac{V_{inj}}{2A_f}\sqrt{\frac{\mu}{\pi k \phi c_t}} \cdot t^{-1/2} \tag{A6}$$

As evident from the above equation, during the linear flow regime, the pressure change is inversely proportional to the square root of time:

$$\Delta P(t) \propto t^{-1/2} \tag{A7}$$

As time progresses and the pressure transient propagates into the far field, the influence of fracture geometry becomes negligible. The fracture effectively degenerates into a line source aligned with the wellbore axis, and the flow evolves into pseudo-radial flow centered on the wellbore [16,17]. In a cylindrical coordinate system, neglecting vertical flow, the diffusion equation is expressed as:

$$\frac{1}{r}\frac{\partial}{\partial r}\left(r\frac{\partial P}{\partial r}\right) = \frac{1}{\eta}\frac{\partial P}{\partial t} \tag{A8}$$

In an infinite formation, the fundamental solution for an instantaneous line source released at $r = 0$ and time $t = 0$ is given by:

$$\Delta P(t) = \frac{S_{line}}{4\pi\eta t} exp\left(-\frac{r^2}{4\eta t}\right) \tag{A9}$$

where S_{line} represents the line source strength, defined as:

$$S_{line} = \frac{V_{inj}/h}{\phi c_t} \tag{A10}$$

For bottomhole pressure measurement, where r is extremely small ($r \to 0$ or $r = r_w$, where r is the radial distance and r_w is the wellbore radius), when time t becomes sufficiently large, the term $exp(-r^2/4\eta t) = 1$, yielding:

$$\Delta P(t) = \frac{V_{inj}\mu}{4\pi kh} \cdot t^{-1} \tag{A11}$$

This indicates that during the pseudo-radial flow regime, the pressure change becomes independent of fracture parameters and is inversely proportional to time:

$$\Delta P(t) \propto t^{-1} \tag{A12}$$

The impulse solution for the pseudo-radial flow regime can be written as:

$$\Delta P(t) = C_r t^{-1} \tag{A13}$$

Similarly, the linear-flow impulse solution can be written as:

$$\Delta P(t) = C_l t^{-1/2} \tag{A14}$$

The derivatives with respect to t are written for after-closure pseudo-radial flow as:

$$-\frac{\partial \Delta P(t)}{\partial t} = C_r t^{-2} \tag{A15}$$

for after-closure linear flow as:

$$-\frac{\partial \Delta P(t)}{\partial t} = \frac{C_l}{2} t^{-3/2} \tag{A16}$$

The semi-logarithmic derivatives are calculated by multiplying the post-shut-in pressure derivatives by time t. Table A1 presents the derivative terms and characteristic slopes for each flow regime.

Table A1. Derivative terms and characteristic slopes for various flow regimes.

Flow Regime	Semilog Derivative	Characteristic Slope
linear	$-t\frac{\partial \Delta P(t)}{\partial t} = \frac{C_l}{2}t^{-1/2}$	$-1/2$
pseudo-radial	$-t\frac{\partial \Delta P(t)}{\partial t} = C_r t^{-1}$	-1

Appendix B

In this study, the processing of pressure falloff data employs the differentiation algorithm proposed by Bourdet [40]. This algorithm computes the pressure derivative at any point i using a weighted mean of the slopes from adjacent data points:

$$\Delta t\frac{dp}{d\Delta t} = \left(\frac{dp}{dln\Delta t}\right)_i = \left(\frac{dp}{dX}\right)_i = \frac{(\Delta p_1/\Delta X_1)\Delta X_2 + (\Delta p_2/\Delta X_2)\Delta X_1}{\Delta X_1 + \Delta X_2} \quad \text{(A17)}$$

where X is explicitly defined as the natural logarithm of the elapsed shut-in time ($X = ln\Delta t$). The variables Δp_1 and Δp_2 represent the pressure differences between point i and the selected preceding (Point 1) and succeeding (Point 2) points, respectively, while ΔX_1 and ΔX_2 denote the corresponding intervals in the logarithmic time domain.

To suppress noise, Points 1 and 2 are not necessarily the immediately adjacent data records. Instead, the algorithm searches backward and forward from point i to select the first points that satisfy a predefined minimum differentiation window, defined as the smoothing parameter L (i.e., $\Delta X_1 \geq L$ and $\Delta X_2 \geq L$).

The parameter L (practically ranging from 0 to 0.5) dictates the trade-off between noise suppression and signal fidelity. A smaller L preserves the original characteristics of the curve, whereas a larger L yields a relatively smoother profile. To optimize this balance for the specific signal characteristics of each dataset, L is set to 0.5 for Case 1 and 0.1 for Case 2 in this study.

References

1. Hottman, C.E.; Johnson, R.K. Estimation of Formation Pressures from Log-Derived Shale Properties. *J. Pet. Technol.* **1965**, *17*, 717–722. [CrossRef]
2. Hubbert, M.K.; Rubey, W.W. Role of fluid pressure in mechanics of overthrust faulting: I. Mechanics of fluid-filled porous solids and its application to overthrust faulting. *Geol. Soc. Am. Bull.* **1959**, *70*, 115–166. [CrossRef]
3. Law, B.E.; Spencer, C.W. Abnormal pressure in hydrocarbon environments. *AAPG Mem.* **1998**, *70*, 1–11. [CrossRef]
4. Sun, S.; Shi, Z.; Dong, D.; Bai, W.; Wei, L.; Yin, J.; Qu, J. Formation and evolution of shale overpressure in deep Wufeng-Longmaxi Formation in southern Sichuan basin and its influence on reservoir pore characteristics. *Front. Earth Sci.* **2024**, *12*, 1375241. [CrossRef]
5. Liu, S.; Yang, X.; Zhao, S.; Xu, H.; Lei, Y.; Liu, Y.; Cao, L.; Li, B.; He, Y.; Xia, Z.; et al. Evaluation of Geo-Engineering Sweet Spots in Deep Shale Gas Reservoirs of the Northern Luzhou Block. *Processes* **2026**, *14*, 594. [CrossRef]
6. Liu, L.; Ding, R.; Chen, E.; Zhang, C. Investigation of the CO_2 Pre-Fracturing Mechanism for Enhancing Fracture Propagation and Stimulated Reservoir Volume in Ultra-Deep Oil Reservoirs. *Energies* **2025**, *18*, 96. [CrossRef]
7. Zheng, X.; Jiang, X.; Zhu, L.; Lu, J.; Qiao, L.; Gao, T.; Zhang, T.; Gu, Z.; Chen, T.; Zhang, X. A Numerical Investigation of Fault Slip Induced by Injection–Production Operations in Oilfields. *Energies* **2026**, *19*, 840. [CrossRef]
8. Ellsworth, W.L. Injection-induced earthquakes. *Science* **2013**, *341*, 1225942. [CrossRef] [PubMed]
9. Li, J.; Zhu, A.; Li, Y.; Cui, G.; Jiang, C. The poroelastic stress and pore pressure effects on delayed seismicity based on fully coupled fluid-solid simulations and rate-and-state friction laws. *Geophys. J. Int.* **2026**, *244*, ggaf536. [CrossRef]
10. Shabangu, P.P.; Magoba, M.; Opuwari, M. Pore Pressure Prediction and Fluid Contact Determination: A Case Study of the Cretaceous Sediments in the Bredasdorp Basin, South Africa. *Appl. Sci.* **2025**, *15*, 7154. [CrossRef]
11. Pennebaker, E.S. An Engineering Interpretation of Seismic Data. In Proceedings of the Fall Meeting of the Society of Petroleum Engineers of AIME, Houston, TX, USA, 29 September–2 October 1968. [CrossRef]
12. Eaton, B.A. The Effect of Overburden Stress on Geopressure Prediction from Well Logs. *J. Pet. Technol.* **1972**, *24*, 929–934. [CrossRef]

13. Feng, J.; Wang, Q.; Li, M.; Li, X.; Zhou, K.; Tian, X.; Niu, J.; Yang, Z.; Zhang, Q.; Sun, M. Pore Pressure Prediction for High-Pressure Tight Sandstone in the Huizhou Sag, Pearl River Mouth Basin, China: A Machine Learning-Based Approach. *J. Mar. Sci. Eng.* **2024**, *12*, 703. [CrossRef]
14. Yang, Y.; Sun, D.; Meng, W.; Li, A.; Wang, B.; Chen, Q. Deep borehole in situ stress measurements by hydraulic fracturing method in Xuefengshan area. *IOP Conf. Ser. Earth Environ. Sci.* **2020**, *570*, 042024. [CrossRef]
15. Nolte, K.G. Determination of fracture parameters from fracturing pressure decline. In Proceedings of the SPE Annual Technical Conference and Exhibition, Las Vegas, NV, USA, 23–26 September 1979. [CrossRef]
16. Soliman, M.Y.; Craig, D.; Bartko, K.; Rahim, Z.; Adams, D. After-Closure Analysis to Determine Formation Permeability, Reservoir Pressure, and Residual Fracture Properties. In Proceedings of the 14th SPE Middle East Oil and Gas Show and Conference, Manama, Bahrain, 12–15 March 2005. [CrossRef]
17. Craig, D.P.; Blasingame, T.A. Application of a New Fracture-Injection/Falloff Model Accounting for Propagating, Dilated, and Closing Hydraulic Fractures. In Proceedings of the SPE Gas Technology Symposium, Calgary, AB, Canada, 15–17 May 2006. [CrossRef]
18. Barree, R.D.; Barree, V.L.; Craig, D.P. Holistic Fracture Diagnostics: Consistent Interpretation of Prefrac Injection Tests Using Multiple Analysis Methods. *SPE Prod. Oper.* **2009**, *24*, 396–406. [CrossRef]
19. Wang, H.; Sharma, M.M. A Novel Approach for Estimating Formation Permeability and Revisit After-Closure Analysis of Diagnostic Fracture Injection Tests. *SPE J.* **2019**, *24*, 1957–1971. [CrossRef]
20. Talley, G.R.; Swindell, T.M.; Waters, G.A.; Nolte, K.G. Field Application of After-Closure Analysis of Fracture Calibration Tests. In Proceedings of the SPE Mid-Continent Operations Symposium, Oklahoma City, OK, USA, 28–31 March 1999. [CrossRef]
21. Nolte, K.G.; Maniere, J.L.; Owens, K.A. After-Closure Analysis of Fracture Calibration Tests. In Proceedings of the SPE Annual Technical Conference and Exhibition, San Antonio, TX, USA, 5–8 October 1997. [CrossRef]
22. Al-Shaikh, A.; Weijermars, R. Fast Analysis Method of Diagnostic Fracture Injection Test Data: Examples from Four Different Shale Formations (Bakken, Three Forks, Wolfcamp, and Eagle Ford). In Proceedings of the SPE International Hydraulic Fracturing Technology Conference and Exhibition, Muscat, Oman, 23–25 September 2025. [CrossRef]
23. Zanganeh, B.; Clarkson, C.R. Pressure Decline Analysis in Fractured Horizontal Wells: Comparison between Diagnostic Fracture Injection Test, Flowback, and Main Stage Falloff. *SPE Drill. Complet.* **2021**, *36*, 717–729. [CrossRef]
24. Clarkson, C.R.; Zeinabady, D.; Zanganeh, B.; Haqparast, S. Learnings from Over 5 Years of Design, Implementation, and Analysis of the Modified Flowback DFIT, DFIT-FBA. In Proceedings of the SPE Hydraulic Fracturing Technology Conference and Exhibition, The Woodlands, TX, USA, 4–6 February 2025. [CrossRef]
25. Wang, H.; Sharma, M.M. Uniquely determine fracture dimension and formation permeability from diagnostic fracture injection test. *Rock Mech. Bull.* **2023**, *2*, 100040. [CrossRef]
26. Belyadi, H.; Fathi, E.; Belyadi, F. Chapter 14—Diagnostic Fracture Injection Test (DFIT). In *Hydraulic Fracturing in Unconventional Reservoirs*; Gulf Professional Publishing: Oxford, UK, 2017; pp. 257–278.
27. Wu, J.; Ren, L.; Chang, C.; Sheng, S.; Zhu, J.; Liu, S.; Xie, W.; Wang, F. Diagnostics of Secondary Fracture Properties Using Pressure Decline Data during the Post-Fracturing Soaking Process for Shale Gas Wells. *Processes* **2024**, *12*, 239. [CrossRef]
28. McClure, M.; Bammidi, V.; Cipolla, C.; Cramer, D.; Martin, L.; Savitski, A.A.; Sobernheim, D.; Voller, K. A Collaborative Study on DFIT Interpretation: Integrating Modeling, Field Data, and Analytical Techniques. In Proceedings of the 7th Unconventional Resources Technology Conference, Denver, CO, USA, 22–24 July 2019. [CrossRef]
29. Yang, Y.; Sun, D.; Ma, X.; Wu, B.; Li, A.; Xu, Q.; Chen, Q. Closure Pressure Diagnostics in Diagnostic Fracture Injection Tests Using G-Function and Total System Stiffness Methods. *SPE J.* **2026**, 1–13. [CrossRef]
30. Qin, X.; Chen, Q.; Zhao, X.; Zhang, C.; Sun, D.; Meng, W.; Feng, C.; Wang, B.; Yang, Y. Experimental study on the crucial effect of test system compliance on hydraulic fracturing in-situ stress measurements. *Chin. J. Rock Mech. Eng.* **2020**, *39*, 1189–1202. [CrossRef]
31. McClure, M.; Fowler, G.; Picone, M. Best Practices in DFIT Interpretation: Comparative Analysis of 62 DFITs from Nine Different Shale Plays. In Proceedings of the SPE International Hydraulic Fracturing Technology Conference & Exhibition, Muscat, Oman, 11–13 January 2022. [CrossRef]
32. Castillo, J.L. Modified Fracture Pressure Decline Analysis Including Pressure-Dependent Leakoff. In Proceedings of the SPE Rocky Mountain Regional Meeting, Casper, WY, USA, 18–20 May 1987. [CrossRef]
33. McClure, M.W.; Jung, H.; Cramer, D.D.; Sharma, M.M. The Fracture-Compliance Method for Picking Closure Pressure from Diagnostic Fracture-Injection Tests. *SPE J.* **2016**, *21*, 1321–1339. [CrossRef]
34. Gabry, M.A.; Eltaleb, I.; Ramadan, A.; Rezaei, A.; Soliman, M.Y. Hydraulic Fracture Closure Detection Techniques: A Comprehensive Review. *Energies* **2024**, *17*, 4470. [CrossRef]
35. Yang, Y.; Sun, D.; Ma, X.; Wu, B.; Chen, Q. A total system stiffness approach for determining shut-in pressure in hydraulic fracturing stress measurements. *Int. J. Rock Mech. Min. Sci.* **2025**, *192*, 106160. [CrossRef]
36. Wang, R.; Dahi Taleghani, A.; Cai, Y. Flowback Rates for Pump-In/Flowback Test. *SPE J.* **2024**, *29*, 3905–3923. [CrossRef]

37. Virues, C.; Robertson, A.; Aboukhalil, E. Best Practices in DFIT Interpretation: Comparative Analysis of 83 DFITs in the Canadian Duvernay Shale Play. In Proceedings of the SPE Annual Technical Conference and Exhibition, Houston, TX, USA, 3–5 October 2022. [CrossRef]
38. Liu, L.; Xue, L.; Han, J. Pressure Transient Analysis for Fractured Shale Gas Wells Using Trilinear Flow Model. *Processes* **2024**, *12*, 2652. [CrossRef]
39. Gringarten, A.C.; Ramey, H.J.; Raghavan, R. Unsteady-State Pressure Distributions Created by a Well with a Single Infinite-Conductivity Vertical Fracture. *SPE J.* **1974**, *14*, 347–360. [CrossRef]
40. Bourdet, D.; Ayoub, J.A.; Plrard, Y.M. Use of Pressure Derivative in Well-Test Interpretation. *SPE Form. Eval.* **1989**, *4*, 293–302. [CrossRef]

Disclaimer/Publisher's Note: The statements, opinions and data contained in all publications are solely those of the individual author(s) and contributor(s) and not of MDPI and/or the editor(s). MDPI and/or the editor(s) disclaim responsibility for any injury to people or property resulting from any ideas, methods, instructions or products referred to in the content.